

SiPM behaviour under continuous light

A. Nagai,^{1,a} C. Alispach,^a D. della Volpe,^a M. Heller,^a T. Montaruli,^a S. Njoh,^a I. Troyano-Pujadas,^a Y. Renier^a

^aDépartement de physique nucléaire et corpusculaire, Université de Genève, 24 Quai E. Ansermet, CH-1211, Switzerland

E-mail: Andrii.Nagai@unige.ch

ABSTRACT: This paper reports on the behaviour of Silicon Photomultiplier (SiPM) detectors under continuous light. Usually, the bias circuit of a SiPM has a resistor connected in series to it, which protects the sensor from drawing too high current. This resistor introduces a voltage drop when a SiPM draws a steady current, when illuminated by constant light. This reduces the actual SiPM bias and then its sensitivity to light. As a matter of fact, this effect changes all relevant SiPM features, both electrical (i.e. breakdown voltage, gain, pulse amplitude, dark count rate and optical crosstalk) and optical (i.e. photon detection efficiency). To correctly operate such devices, it is then fundamental to calibrate them under various illumination levels.

In this work, we focus on the large area ($\sim 1 \text{ cm}^2$) hexagonal SiPM S10943-2832(X) produced by Hamamatsu HPK for the camera of a gamma-ray telescope with 4 m-diameter mirror, called the SST-1M. We characterize this device under light rates ranging from 3 MHz up to 5 GHz of photons per sensor at room temperature ($T = 25 \text{ }^\circ\text{C}$). From these studies, a model is developed in order to derive the parameters needed to correct for the voltage drop effect. This model can be applied for instance in the analysis of the data acquired by the camera to correct for the effect. The experimental results are also compared with a toy Monte Carlo simulation and finally, a solution is proposed to compensate for the voltage drop.

KEYWORDS: SiPM, voltage drop, SST-1M, *PDE*, crosstalk, dark count rate, afterpulses, triggering probability, night sky background (NSB) and continuous light.

¹Corresponding author.

Contents

1	Introduction	1
2	SiPM behaviour under continuous light	2
3	Analytic description of the voltage drop process	4
4	The toy Monte Carlo	7
5	Validation of the toy Monte Carlo	9
5.1	Validation with the analytical calculation	9
5.2	Validation with calibrated light sources	10
5.3	Validation with the Camera Test Setup	14
6	Results	14
7	Conclusions	16

1 Introduction

SiPM detectors have become the preferred photosensors for many applications in high-energy particle and astroparticle physics, and they are very attractive also for LIDAR and medical imaging applications for diagnostic and therapeutic purposes. More traditionally, such applications employ photomultiplier tubes (PMTs) or multi-anode PMTs (MA-PMTs). Between the important advantages of SiPMs there are compactness, speed of response, insensitivity to magnetic fields, high gain, and low operating voltage. Additionally, with respect to PMTs, they offer the possibility to operate under high and continuous illumination without ageing. While SiPM devices are commonly used as single photon detectors operating in dark conditions, in this study we describe how SiPM devices can be used as multi-photon detectors under continuous light (CL).

As an example application of SiPM in the presence of CL, SiPMs are now being adopted for cameras of Imaging Atmospheric Cherenkov Telescopes (IACTs) dedicated to gamma-ray astronomy. The pathfinder of this technology applied to gamma-ray astronomy has been the FACT telescope [1]. Further developments have been performed for the implementation of the Cherenkov Telescope Array (CTA) [2, 3], in the frame of which the SST-1M was originally developed [4] with its SiPM-based camera [5]. Thanks to their robustness, the CL at which SiPMs can operate is higher than for photomultipliers [6]. For IACTs, CL is due to night sky background (NSB), meaning stray light from reflections from ground and light from human induced sources, and light due the presence of high moon.

Continuous light on a SiPM sensor leads to a steady current flowing through it. To prevent such a high current to eventually damage it, a bias resistor, R_{bias} , is connected in series with the

SiPM. This current flowing in R_{bias} translates into a voltage drop V_{drop} at the SiPM bias stage thus reducing the current. It is a typical negative feedback loop. At the same time, the V_{drop} affects the over-voltage, $\Delta V = V_{BD} - V_{PS}$ (where V_{BD} is the breakdown voltage and V_{PS} the bias voltage supplied by the power supplier PS), which impacts most of the SiPM parameters: gain (G), timing, photon detection efficiency (PDE), dark count rate (DCR), optical crosstalk probability (P_{ct}) and afterpulse probability (P_{ap}). Therefore, when SiPM devices are used in the presence of CL, all these parameters have to be characterized as a function of the impinging light intensity to correctly define the performance of a sensor. The consequence of the variation of SiPM operation parameters is that the same incoming physics signal produces a different output when observed in different CL levels. At the analysis level, the corrections for this effect must be applied to interpret experimental data properly. These corrections are important for the operation of SiPM-based gamma-ray cameras and also for applications where sensors are subject to high radiation levels, which induce an increasing dark count rate with increasing integrated dose. In this case, the dark count rate can reach such high levels to mimic CL with rates of the order of several MHz [7].

In Sec. 2 we illustrate further the behaviour of SiPM devices under CL. In Sec. 3 we describe the voltage drop process mathematically and in Sec. 4 we describe the implementation of a toy Monte Carlo (MC) for DC coupled electronics systems. After, in Sec. 5 we show the comparison of the proposed toy MC model with the simplified analytical calculation and with measurements obtained in the laboratory with a calibrated light source (Sec 5.2) and with the SST-1M camera and its Camera Test Setup (see Sec. 5.3).

2 SiPM behaviour under continuous light

In this section, we describe how SiPM devices can also be used as multi-photon detectors under CL. In this paper we focus on a DC coupled electronics associated to the SiPM.

Typical digitized experimental waveforms obtained in dark conditions and under two levels of CL are presented in Fig. 1-left, while the corresponding amplitude W_i distribution is shown in Fig. 1-right. In dark conditions, the number of generated avalanches N_{av} can be calculated by simple counting of SiPM pulses. However, above a given level of CL intensity, SiPM pulses become indistinguishable. This happens when the pulse duration of a single photon becomes compatible with the time lapse between 2 photons, i.e. the photon rate. Therefore the counting of SiPM pulses becomes impossible. Nevertheless, under high CL, N_{av} can be approximated by:

$$N_{av} = \frac{BLS \times \Delta t}{Q_{1pe}} \quad (2.1)$$

where Q_{1pe} is the integral of the single p.e. pulse over its pulse length, Δt is the waveform length and BLS is the baseline shift calculated as:

$$BLS = \frac{1}{S} \left(\sum_{i=0}^{S-1} W_i(\Delta V > 0) - \sum_{i=0}^{S-1} W_i(\Delta V < 0) \right) \quad (2.2)$$

where $W_i(\Delta V > 0)$ and $W_i(\Delta V < 0)$ are the amplitude values of the experimental waveforms for a given sample i acquired with the SiPM biased above the breakdown voltage V_{BD} and below, respectively, and S is the number of waveform samples. It is worth to mention that $W_i(\Delta V < 0)$ is

dominated by the electronics baseline, while $W_i(\Delta V > 0)$ contains also both detected light pulses (if the SiPM is exposed to light) and SiPM correlated noise. Correlated noise is due to afterpulses and cross-talk. There is a given probability that an afterpulse might generate itself other afterpulses, P_{ap} . Therefore, following the Ref. [8], the total probability that an initial avalanche will be enhanced by afterpulses is:

$$P_{ap,tot} = P_{ap} + P_{ap}^2 + P_{ap}^3 + \dots = \frac{P_{ap}}{1 - P_{ap}} \quad (2.3)$$

Similarly, for optical cross-talk, with a given probability P_{ct} , this enhancement of the cascading effect leads to:

$$P_{ct,tot} = P_{ct} + P_{ct}^2 + P_{ct}^3 + \dots = \frac{P_{ct}}{1 - P_{ct}} \quad (2.4)$$

The N_{av} is the number of avalanches due to the detected photons and augmented by SiPM correlated and uncorrelated noise:

$$N_{av} = (N_{pe} + DCR \times \Delta t) \cdot (1 + P_{ct,tot}) \cdot (1 + P_{ap,tot}) \quad (2.5)$$

where N_{pe} is the number of detected photons. Therefore, N_{pe} , can be calculated as:

$$N_{pe} = \frac{N_{av} - DCR \times \Delta t}{(1 + P_{ct,tot}) \times (1 + P_{ap,tot})}, \quad (2.6)$$

and the number of photons N_{ph} can be calculated as:

$$N_{ph} = \frac{N_{pe}}{PDE}. \quad (2.7)$$

Usually SiPMs are operated in dark conditions and therefore also PDE and noise, namely, DCR , P_{ct} and P_{ap} , are evaluated in dark conditions. Nonetheless, SiPMs are usually biased through a RC filter (see e.g. [9]) in order to:

- filter high frequency electronic noise coming from the bias source;
- limit the current in order to protect the sensor in case of intense illumination.

Due to the presence of the bias resistor R_{bias} and CL, the SiPM parameters deviate from their "dark" values, meaning their values measured in dark conditions. As a matter of fact, the voltage drop, V_{drop} , induced by the bias resistor R_{bias} reduces the over-voltage ΔV as follows:

$$\Delta V = V_{PS} - V_{BD} - V_{drop} = V_{PS} - V_{BD} - R_{bias} \times I_{SiPM} \quad (2.8)$$

where I_{SiPM} is the current generated by the SiPM. From Eq. 2.8, one can conclude that the smaller R_{bias} is, the more stable will be the sensor response. However, having a small R_{bias} also means that high currents can flow through a SiPM, leading to self-heating of the sensor for high CL, as shown in Fig. 2. If there is a possibility to measure the I_{SiPM} , the V_{drop} can be compensated by the feedback system described in Ref. [10]. For other cases, the I_{SiPM} can be calculated analytically or from the toy MC, as shown in next sections.

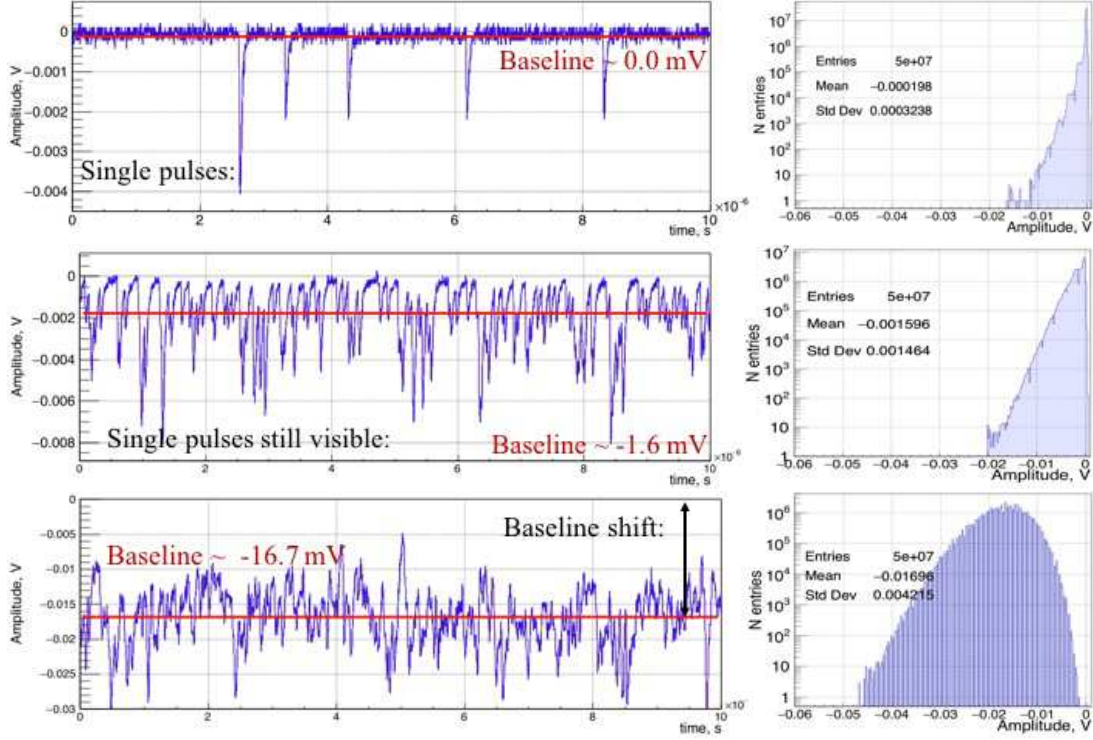


Figure 1: From top to bottom: Typical response (waveform) of SiPM in dark conditions (3 MHz DCR), under illumination with photon rates of 40.9 MHz and 660 MHz. The amplitude distribution for 10'000 waveforms is shown on the right side for each light intensity level.

3 Analytic description of the voltage drop process

The voltage drop process can be described by the scheme in Fig. 3. We adopt in the figure the already defined voltage supplied by the power supply, V_{PS} , the breakdown voltage V_{BD} and the one at the SiPM terminals V_{SiPM} . The rates of CL expressed in photons and in photo-electrons (p.e.) per unit of time are, respectively, F_{ph} and F_{pe} (where F_{pe} is obtained from F_{ph} at a certain wavelength using the PDE). The important input parameters for this model are:

- the microcell $C_{\mu cell}$ and parasitic C_q capacitance's, which determine the SiPM gain, $G = (C_{\mu cell} + C_q) \cdot \Delta V / e$, and therefore allow to convert p.e. to current;
- the $PDE(\lambda, \Delta V)$ determines the probability that a photon of a given wavelength is detected at a given over-voltage ΔV ;
- DCR determines the rate of thermally generated avalanches at a given ΔV (i.e. the uncorrelated SiPM noise);
- The optical crosstalk probability, P_{ct} and the after pulse probability, P_{ap} (i.e. the correlated SiPM noise). Both probabilities enhance the total rate of avalanches produced by SiPM at a given ΔV ;
- a precise template of the typical normalized SiPM pulse due to 1 p.e. at a given temperature. The SiPM pulse template can be calculated by averaging a given number of normalized

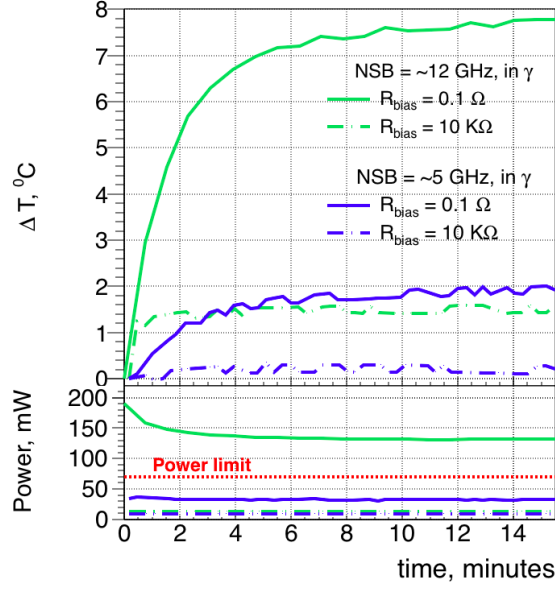


Figure 2: SiPM temperature (upper panel) and power consumption (bottom panel) at initial $\Delta V = 2.8$ V and under 12×10^9 photons/s vs time for $R_{bias} = 0.1 \Omega$ (solid line) and $R_{bias} = 10 \text{ k}\Omega$ (dashed line). The highest acceptable power consumption for the sensor (provided by the producer) is represented by the red dashed line.

single ¹ pulses. Special care is taken in retrieving the slow component of the pulse. Even if its contribution to the total charge is small (e.g. $< 1\%$), with rates up to few GHz, neglecting it would lead to large discrepancies on the waveform baseline shift, which is used to derive the level of CL². See Sec. 5.2 for more information about how to compensate for the slow component of the pulse.

Apart from $C_{\mu cell}$, all aforementioned parameters depend on ΔV and are therefore effected by the voltage drop V_{drop} .

The calculation and simulation of the voltage drop requires to calculate dynamically the current generated by the SiPM:

$$I_{SiPM} = F_{av} \times \frac{(C_{\mu cell} + C_q) \cdot \Delta V}{e} \quad (3.1)$$

with ΔV given by Eq. 2.8. The total rate of avalanches produced by the detected light enhanced by correlated and uncorrelated noise F_{av} , is given by:

$$F_{av} = (DCR + F_{ph} \cdot PDE) \cdot \left(1 + \frac{P_{ct}}{1 - P_{ct}}\right) \cdot \left(1 + \frac{P_{ap}}{1 - P_{ap}}\right) \quad (3.2)$$

¹A single p.e. pulse is separated by neighboring pulses by a time interval longer than the sum of the typical SiPM rise and recovery times.

²CL is provided by NSB in the case of gamma-ray cameras.

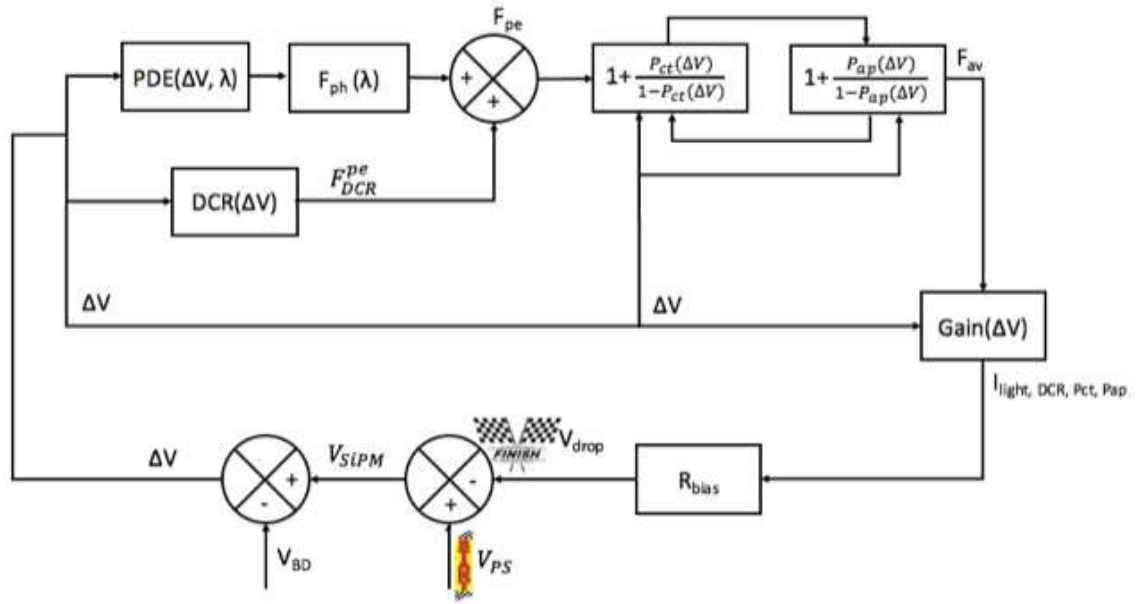


Figure 3: Representation of the impact of CL on the voltage applied to the sensor. The first loop starts at the START on the bottom, where the V_{PS} is provided to the sensor. The overvoltage is then estimated $\Delta V = V_{PS} - V_{BD}$ and the total rate of avalanches F_{av} is calculated from the injected CL (F_{ph}) rate (transformed into p.e. using the PDE and adding uncorrelated noise DCR). This p.e. rate is enhanced by correlated noise (i.e. optical crosstalk P_{ct} and afterpulses P_{ap}). F_{av} produces the current I_{light} after multiplying by the gain. This current is flowing through the bias resistor R_{bias} and decreases the voltage applied by the user V_{PS} down to V_{SiPM} , which is seen by the SiPM. This causes a drop of the values of G , PDE , DCR , P_{ct} , P_{ap} and the loop can restart.

Following Ref. [11], PDE , P_{ct} , P_{ap} and DCR can be parameterized as:

$$PDE = PDE_{max} \cdot P_G \quad (3.3)$$

$$P_{ct} = G \cdot P_{hv} \cdot P_G^{XT} \quad (3.4)$$

$$P_{ap} = G \cdot P_{trap} \cdot P_G^{PAP} \quad (3.5)$$

$$DCR = N_{car} \cdot P_G^{PDCR} \cdot e^{b \cdot V_{SiPM}}, \quad (3.6)$$

where PDE_{max} is a free parameter, which depends on the SiPM type, the light wavelength and, to some extent, on the temperature; P_G , P_G^{XT} , P_G^{PAP} and P_G^{PDCR} are the average Geiger probabilities for external light of a given wavelength, optical crosstalk, after-pulses and dark pulses, respectively, and P_{trap} is the probability that a carrier is trapped and released after; P_{hv} is the probability that a photon is emitted and reaches the high field region of another μ cell and creates an electron-hole pair; N_{car} is the rate of thermally generated carriers; b is another free parameter describing the increase of DCR with V_{SiPM} due to electrical field effects.

Eq. 3.1 becomes non-linear, once taking into account Eq. 2.8 and Eqs. 3.2–3.6. In order to simplify Eq. 3.1, the Taylor series expansion can be applied to Eq. 3.2-3.6. However, to achieve a reasonable agreement between the formula and the measured parameters (i.e. PDE , P_{ct} , P_{ap} and

DCR), the Taylor expansion needs a second or even third terms, which eventually leads to a fifth order in Eq. 3.1.

An analytical calculation of Eq. 3.1 can be done only for the simplified case that CL affects only the SiPM gain G [12], while all other parameters (i.e. PDE , DCR , P_{ct} and P_{ap}) are not affected. This allows to express the voltage drop as a function of the CL rate as follows:

$$V_{drop} = \Delta V - \frac{\Delta V}{1 + R_{bias} \cdot F_{pe} \cdot C_{\mu cell}} \quad (3.7)$$

where F_{pe} is the CL rate expressed in p.e. per second.

To have a precise calculation of V_{drop} and at the same time avoid the complexity of solving Eq. 3.1 analytically, a toy MC model is developed.

4 The toy Monte Carlo

The described model in Sec. 3 is implemented into a toy MC. In the first step, all relevant SiPM parameters are measured experimentally for the large area ($\sim 1 \text{ cm}^2$) hexagonal SiPM, S10943-2832(X), produced by Hamamatsu HPK [9] for the single mirror small size telescope SST-1M camera. All these parameters and their measurements are described in Ref. [11].

Each simulated time interval, typically between 200 and 2'000 ns, was sampled with a given sampling rate R_s and sample time width $\Delta t_i = 1/R_s$ (typically, in the interval $100 \text{ ps} \leq \Delta t_i \leq 4 \text{ ns}$). For each sample i , in the range from 0 to $S - 1$, the main simulation steps are:

1. randomly generate a number of photons $N_{gen}(\lambda, i)$ using a Poisson distribution with mean value of $F_{ph}(i) \cdot \Delta t_i$ according to the CL rate with a given wavelength distribution or single wavelength. If the simulated optical system contains wavelength filters, e.g. entrance window of the camera with anti-reflective coating and low pass filter, it can be accounted for at this stage;
2. each generated photon is processed separately. It may be detected or not, depending on the PDE and photon wavelength:

$$N_{light}^{p.e.}(i) = \sum_{n=1}^{N_{gen}(\lambda, i)} f(r_n) \quad (4.1)$$

where r is a random number uniformly distributed from 0 to 1 and $f(r)$ is:

$$f(r) = \begin{cases} 1 & \text{if } r \leq PDE(\Delta V(i), \lambda) \\ 0 & \text{if } r > PDE(\Delta V(i), \lambda) \end{cases} \quad (4.2)$$

3. on top of the CL (i.e. $N_{gen}(\lambda, i)$), the SiPM uncorrelated noise (with rate DCR) is added:

$$N_{tot}^{p.e.}(i) = N_{light}^{p.e.}(i) + N_{DCR}(i, r) \quad (4.3)$$

where N_{DCR} is the number of dark pulses, calculated as:

$$N_{DCR}(i, r) = \begin{cases} 1 & \text{if } r \leq DCR(i, \Delta V) \cdot \Delta t_i \\ 0 & \text{if } r > DCR(i, \Delta V) \cdot \Delta t_i \end{cases} \quad (4.4)$$

Here, we neglect that two or more dark pulses may appear within the same Δt_i , because even for large Δt_i of 4 ns this probability is less than 1%.

4. $N_{tot}^{p.e.}(i)$ are randomly enhanced by optical crosstalk and/or afterpulses. The total number of avalanches for a given sample i , is then: $N_{av}(i)$;
5. randomly create an avalanche generation time t_{av} from an uniform distribution in the range $10 \text{ ps} + (i \times \Delta t_i) \leq t_{av} < \Delta t_i \times (i + 1)$;
6. $N_{av}(i)$ is converted into the SiPM current $I_{SiPM}(i)$ as:

$$I_{SiPM}(i) = F_{av}(i) \times \frac{C_{\mu cell} \cdot \Delta V(i)}{e} = \frac{N_{av}(i)}{\Delta t_i} \times G(\Delta V(i)). \quad (4.5)$$

In this step $G(\Delta V(i))$ is randomly smeared with a Gaussian distribution with standard deviation σ_G corresponding to the SiPM gain fluctuation between different micro-cells;

7. $I_{SiPM}(i)$ is used to calculate $V_{drop}(i)$, and both are used to estimate the effect on the over-voltage in the sample $i + 1$:

$$\Delta V(i + 1) = \Delta V(i) - V_{drop}(i) \quad (4.6)$$

The overvoltage $\Delta V(i + 1)$ is used to derive the values of all parameters (e.g. G , $A_{p.e.}$, PDE , DCR , P_{ct} and P_{ap}) for the sample $i + 1$;

8. the arrival time of detected and generated photons, as well as all parameters used in the simulation, are stored in a ROOT³ binary file for future use.

At the last sample $i = S - 1$, the experimental waveform is generated as the sum of all the generated avalanches $N_{av}(i)$ convoluted with the template of the typical normalized SiPM pulse with its amplitude $A_{p.e.}(\Delta V(i), i)$ and shifted by the initial electronic baseline. Additionally, each waveform value is randomly smeared by a Gaussian distribution with a standard deviation σ_e corresponding to the electronic noise of the system under consideration.

To illustrate the simulation steps, the average I_{SiPM} resulting from the simulation of a SiPM illuminated with a photon rate of $F_{ph} = 2 \text{ GHz}$ as a function of time is presented in Fig. 4 (top) for two values of R_{bias} of 2.4 k Ω and 10 k Ω . Relatively fast changes of the main SiPM parameters, in particular of the over-voltage ΔV , and consequently of the PDE , are observed within the first time steps of the simulation before the steady state is reached. Such a behaviour is related to recursive conjugation of I_{SiPM} and ΔV . At $t = 0$, I_{SiPM} increases with N_{av} (see Eq. 3.1), but it is quickly quenched by the presence of the bias resistor which causes the over-voltage to decrease (See Eq. 2.8). The time interval before the steady state is achieved increases with F_{ph} and G . For this particular example, it is reached after $\sim 100 \text{ ns}$.

³<https://root.cern.ch>

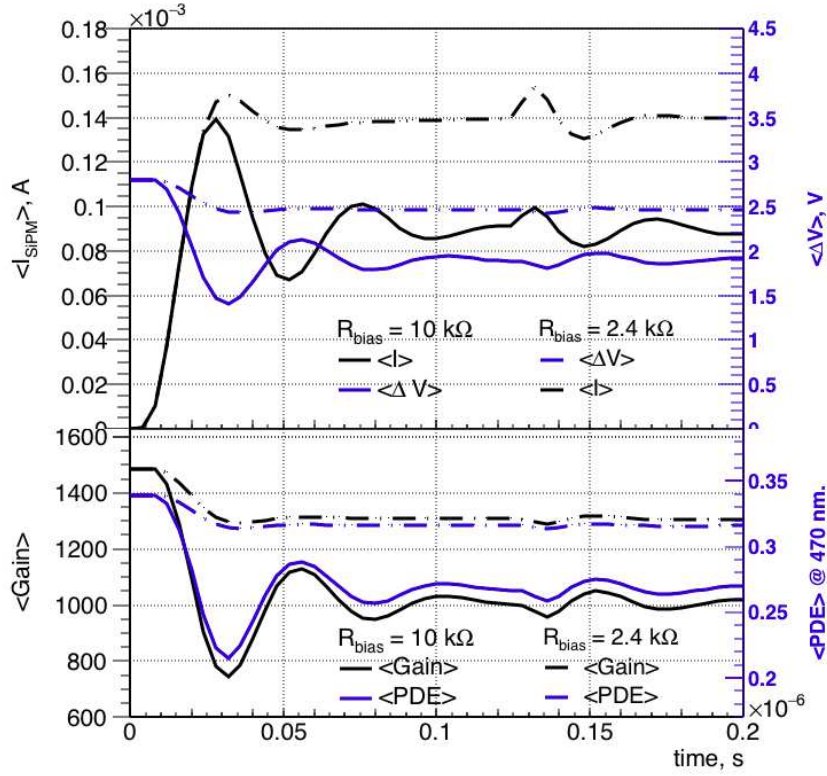


Figure 4: The simulated current in a SiPM, I_{SiPM} , vs time under CL with photon rate of 2 GHz. I_{SiPM} induces a drop of ΔV , which in turn affects all main SiPM parameters (i.e. G , PDE , P_{ct} , P_{ap} and DCR). As an example the PDE and G as a function of time are presented in the bottom plot. Results are presented for two values of R_{bias} of 10 k Ω and 2.4 k Ω .

5 Validation of the toy Monte Carlo

The proposed toy MC is compared with a simplified analytical calculation [12], and then with measurements obtained in the laboratory with a calibrated light source. It is then compared with data taken with the SST-1M camera and its Camera Test Setup (CTS) [5]. The results are described below.

5.1 Validation with the analytical calculation

As discussed in Sec. 3, the analytical calculation of voltage drop can be done assuming that CL affects only the SiPM gain G . To compare this analytic expression with the proposed toy MC, the voltage drop is simulated using real SiPM parameters and using a simplified case. For this simplified case, we use the toy model assuming null values for DCR , P_{ct} and P_{ap} and that the PDE is 100%. The results for $R_{bias} = 10 \text{ k}\Omega$ (full symbols) and 2.4 k Ω (empty symbols) are presented in Fig. 5. Independently of R_{bias} , the comparison between the analytical expression (lines) and the simplified model (squares) shows an excellent agreement. The relative difference is less than 0.5% on average. When compared to the full model (circles), the relative difference increases to

an average of $\sim 14\%$, which is expected due to the assumed simplifications to use the analytical expression.

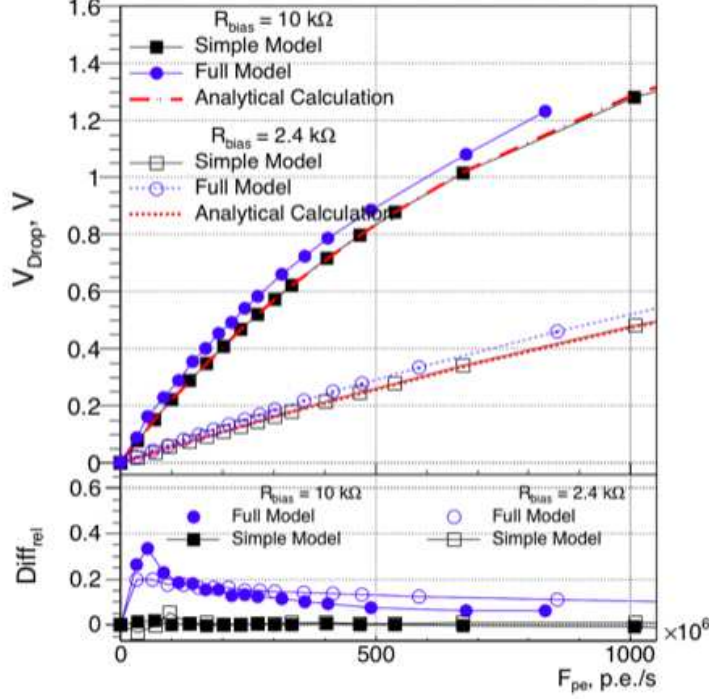


Figure 5: V_{drop} as a function of F_{pe} , calculated analytically (red line), with the simplified toy MC (which assumes $PDE = 100\%$, $DCR = 0$, $P_{ap} = 0$, $P_{ct} = 0$) (black squares) and with the toy MC with real SiPM parameters ($PDE(\Delta V)$, $P_{ct}(\Delta V)$, $P_{ap}(\Delta V)$ and $DCR(\Delta V)$) (blue circles). Results are for two values of R_{bias} of 10 k Ω (closed symbols) and 2.4 k Ω (open symbols).

5.2 Validation with calibrated light sources

For this study, the experimental setup at IdeaSquare⁴ at CERN was used, and is illustrated in Fig. 6. The full description of the set-up may be found in [11]. The SiPM is biased with a Keithley 2410 through an RC filter ($R_{bias} = 10$ k Ω , $C_{bias} = 100$ nF). The SiPM anode is connected to the Keithley Picoammeter 6487 to measure the bias voltage at the SiPM and also to the preamplifier board developed for the SST-1M camera (more details can be found in [5, 12]). The waveform readout is performed with a Lecroy 620Zi oscilloscope. The set-up is equipped with two LEDs ($\lambda = 470$ nm each). A LED is pulsed in AC mode (to emulate the flashes of Cherenkov light induced by atmospheric showers), while the other is continuous, or in the so-called DC mode (to emulate the NSB or CL). The SiPM under study was biased to $V_{PS} = 58$ V and temperature of 25 $^{\circ}$ C, corresponding to $\Delta V = 3.22$ V. For each light level, 10⁵000 waveforms are acquired, each of 2 μ s

⁴<http://ideasquare.web.cern.ch>

long (5'000 samples per waveform). The light intensity is monitored with 5% precision using a calibrated photodiode⁵. Two types of measurements were performed, as described next.

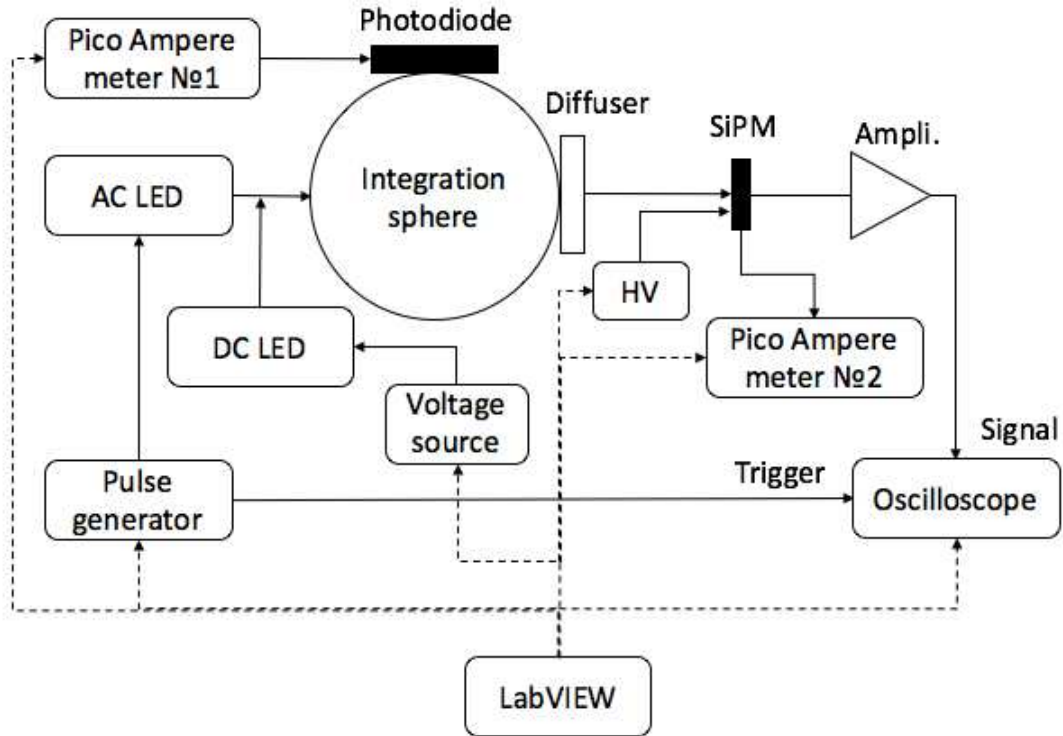


Figure 6: Schematic layout of the experimental set-up used for the toy model validation. Two LEDs are used, one in AC mode to emulate the signal and another in DC mode to emulate various CL levels. The light intensity is measured by the calibrated photodiode. An additional pico-amperometer is used to directly measure the voltage drop and an oscilloscope is used for data acquisition.

DC scan The first measurement is performed with different CL levels. The LED in continuous mode is used to emulate the various CL levels. The measured $V_{drop} = V_{PS} - V_{SiPM}$ and average waveform baseline are compared with simulated values. Fig. 7-left shows a good agreement between the measured and the simulated V_{drop} as a function of F_{ph} in terms of photons/s (the number of photons can be extracted using the calibrated photodiode). However, the measured baseline shift is almost two times higher with respect to the simulated one (see Fig. 7-right).

The difference in baseline shift can be explained by the slow pulse component (referred to as “DC pulse component”), which extends over 150 ns. This DC pulse component is not included directly in the toy model, as the adopted pulse template is only 150 ns long. The DC pulse component is difficult to measure because of the high DCR and P_{ap} in this large SiPM area (93.6 mm²). Therefore, the DC pulse component is measured using low rates of injected light ($F_{ph} < 120$ MHz). This light level is chosen to fulfill two requirements:

⁵Hamamatsu S1337-1010BQ, s/n 61

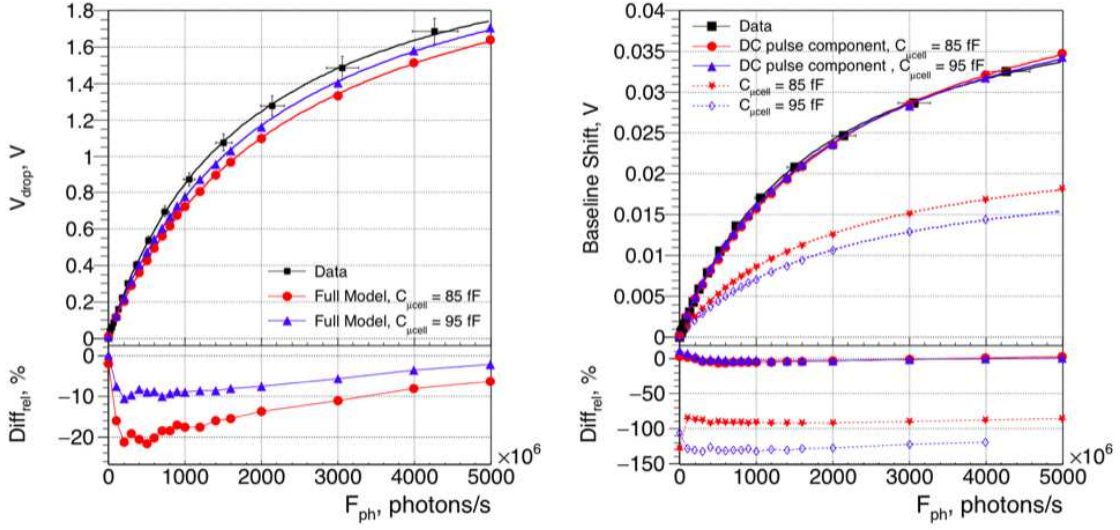


Figure 7: Voltage drop (left) and baseline shift (right) as a function of the CL level in photons per second. Data (black rectangles) are compared to the toy MC assuming two values of $C_{\mu cell}$ of 85 fF (red) and 95 fF (blue). This 85 fF capacitance value was provided by the producer, but we also use 95 fF because of possible 10% parasitic capacitance. The results for the baseline shift from the toy MC is presented with (solid lines) and without correction (dashed lines) for the DC pulse component.

- single SiPM pulses are still distinguishable ⁶;
- the PDE , used to convert F_{ph} into F_{pe} can be considered constant⁷.

For each pulse, the local baseline is calculated within 40 ns before the pulse. The deviation of the local baseline, at a given F_{ph} level, from its value in the dark is called in the following “local baseline shift”: V_{BLS} . The V_{BLS} is converted from a voltage into a charge as:

$$Q_{BLS} = \frac{V_{BLS} \cdot \Delta t}{R_{load}} \quad (5.1)$$

where Δt is the waveform duration and $R_{load} = 50 \Omega$ is the load resistance. At the same time, F_{ph} is converted from number of photons into SiPM detected charge as:

$$Q_{ph} = F_{ph}(\lambda) \cdot PDE(\Delta V, \lambda) \cdot \Delta t \cdot \frac{C_{\mu cell} \cdot \Delta V}{e} \quad (5.2)$$

The average Q_{BLS} as a function of the Q_{ph} is presented in Fig. 8. We can see that the Q_{BLS} increases linearly with Q_{ph} with a slope of $BL_{slope} = 2.1$. This slope indicates that only 32.3% of the charge generated by the SiPM is seen as a pulse, while the remaining 67.7% goes into the

⁶A single pulse is a SiPM signal separated by the neighboring pulses by a time interval higher than $\Delta t_{length} = \Delta t_{rec.} + \Delta t_{rise} + \Delta t_{baseline}$, where $\Delta t_{rec.}$ and Δt_{rise} are the typical SiPM recovery and rise times, respectively, and $\Delta t_{baseline} = 40$ ns is the time interval during which the local baseline calculation is performed.

⁷We estimated a relative PDE drop of 1.75 % for $F_{ph} = 120$ MHz.

baseline shift. Implementing this behaviour inside the toy MC dramatically increases the simulation time. Therefore, the effect is accounted for some additional steps after the simulation is performed. As a matter of fact, each simulated waveform is shifted by an additional baseline BL_{add} , calculated as:

$$BL_{add} = R_{load} \cdot BL_{slope} \cdot \frac{\sum I_{SiPM}}{\Delta t}, \quad (5.3)$$

where $\sum I_{SiPM}$ is the total current generated by the SiPM within the simulated waveform. The results obtained accounting for this additional baseline shift are presented in Fig. 7 (right) with solid lines and indicated as “DC pulse component” in the legend.

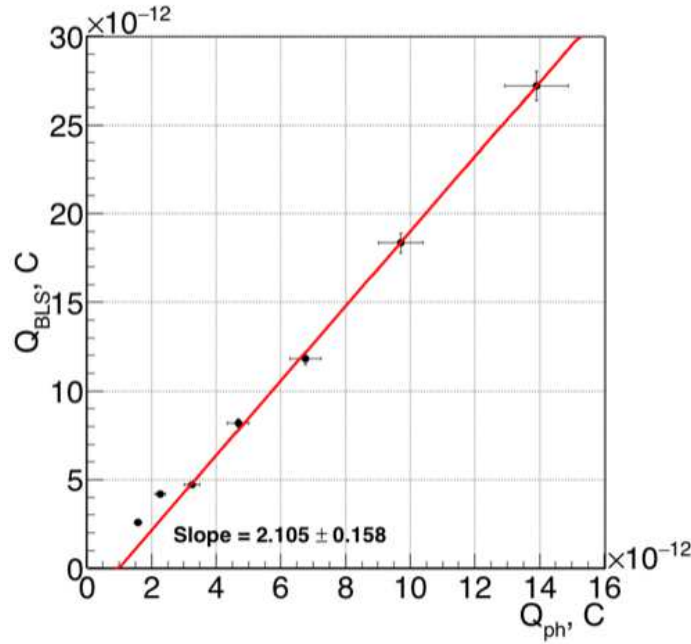


Figure 8: DC pulse component, expressed in baseline shift charge Q_{BLS} as a function of generated SiPM charge Q_{ph} , due to CL.

AC/DC scan The second measurement is performed with different pulsed and CL levels. The average waveform amplitude, A , and average waveform baseline, BL , corresponding to the AC LED, depend on F_{ph} due to the voltage drop effect. The variation with respect to the case without CL can be calculated as:

$$A_{rel} = \frac{A(F) - BL(F)}{A(F0) - BL(F0)} \quad (5.4)$$

where $A(F)$ and $BL(F)$ are the average amplitude and average baseline, respectively, at a given DC LED intensity, while $A(F0)$ and $BL(F0)$ are corresponding values at zero DC intensity. As shown in Fig. 9-left, we can observe that the detected pulse amplitude after baseline subtraction decreases with increasing DC LED intensity, as it is expected due to V_{drop} . This behaviour was compared

with the results from the toy model for $C_{\mu cell}$ of 85 and 95 fF. We can observe that the maximum difference between measured and simulated values, for $C_{\mu cell} = 95$ fF, is less than 5%.

Typically, during the operation of SiPMs in real conditions, the CL level is unknown. However, it can be calculated from the baseline shift or its standard deviation. For these purposes the relative amplitude, $A_{rel.}$, as a function of the baseline shift is presented in Fig. 9-right.

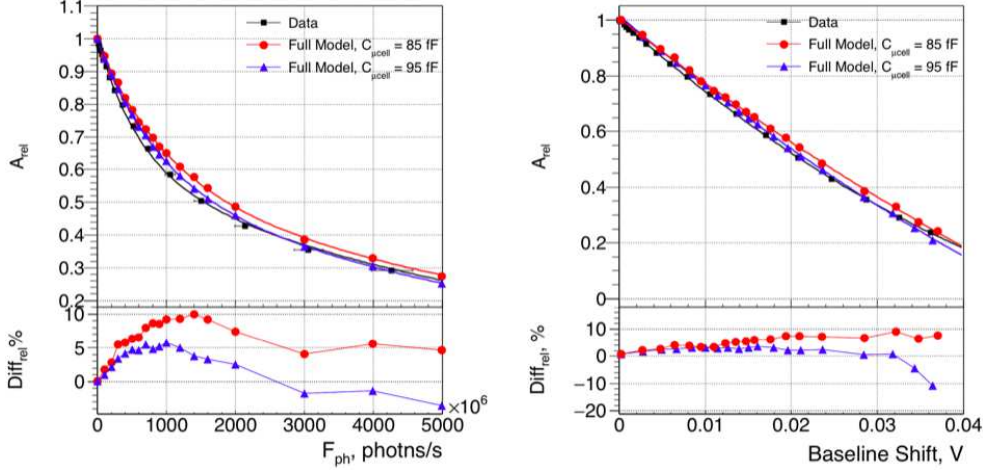


Figure 9: Relative amplitude $A_{rel.}^{Signal}$ from measurements in the laboratory with calibrated light sources (black squares) and from proposed toy MC simulation (red circles for $C_{\mu cell} = 85$ fF and blue triangles for 95 fF) as a function of CL photon rate (left) and baseline shift (right). The relative difference in the relative amplitude for data and simulation is presented in the bottom plots.

5.3 Validation with the Camera Test Setup

Further measurements are performed with the SST-1M camera [5] and its camera test setup (CTS), at the University of Geneva. The CTS calibration tool, described in Ref. [5], is equipped with two LEDs ($\lambda = 468$ nm) corresponding to each SST-1M camera pixel: one in pulsed mode (AC LED) and the other in continuous mode (DC LED). With the CTS, the AC/DC scan described in Sec. 5.2 is done for all 1296 camera pixels at $\Delta V = 2.8$ V. For each pixel, AC and DC LED values, the baseline and signal amplitude are calculated. The relative amplitude (see Eq. 5.4) as a function of the baseline shift is presented in Fig. 10. We can observe that almost for all pixels $A_{rel.}$ decreases with increasing baseline shift (i.e. CL). Few pixels do not follow this tendency as either the pixel itself or the LEDs facing it were found to be faulty. In addition, some LEDs have a higher intensity with respect to others resulting in the saturation of the pixel readout chain [12]. Therefore, no drop of $A_{rel.}$ is observed. The relative difference between data and the proposed model is shown in Fig. 10 (bottom). It is around 5%, confirming the results shown in the previous section.

6 Results

From the proposed toy model, the CL level and the V_{drop} can be obtained from the baseline shift or its standard deviation. Therefore, all SiPM parameters can be corrected according to V_{drop} , as

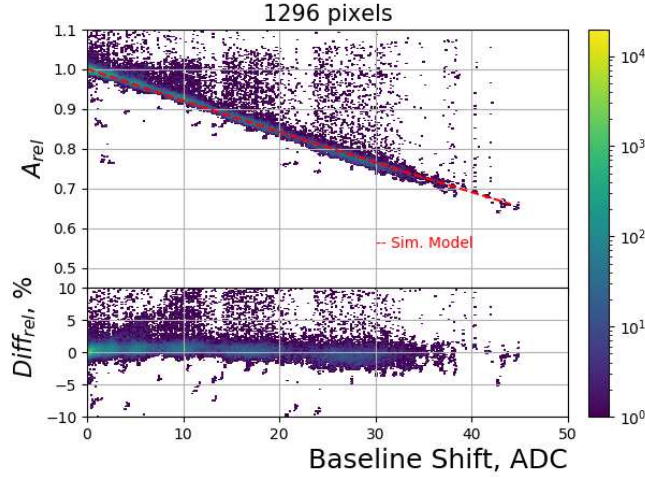


Figure 10: DC/AC scan using 12 different continuous light levels (*DC* LED DAC) and injecting for each CL 19 *AC* LED DAC level pulses. The relative amplitude A_{rel} for all 1296 camera pixels is shown as a function of Baseline shift. The A_{rel} from the proposed model in this paper is represented by the dashed red line. The relative difference in the relative amplitude for data and simulation is presented in the bottom plots.

shown in Fig. 11 for the PDE , P_{ct} and the amplitude of the single p.e. signal. By comparing the relative drop of the main SiPM parameters with CL for R_{bias} of 10 k Ω and 2.4 k Ω we can conclude that for R_{bias} of 2.4 k Ω the relative drop is more than three times smaller, because V_{drop} is proportional to R_{bias} (See Eq. 2.8). Hence, low values of R_{bias} simplify operation of SiPM under CL. A similar plot can be obtained in photons/s when the effect of PDE and additional optical elements (light guides, window, etc.) are included in the simulation.

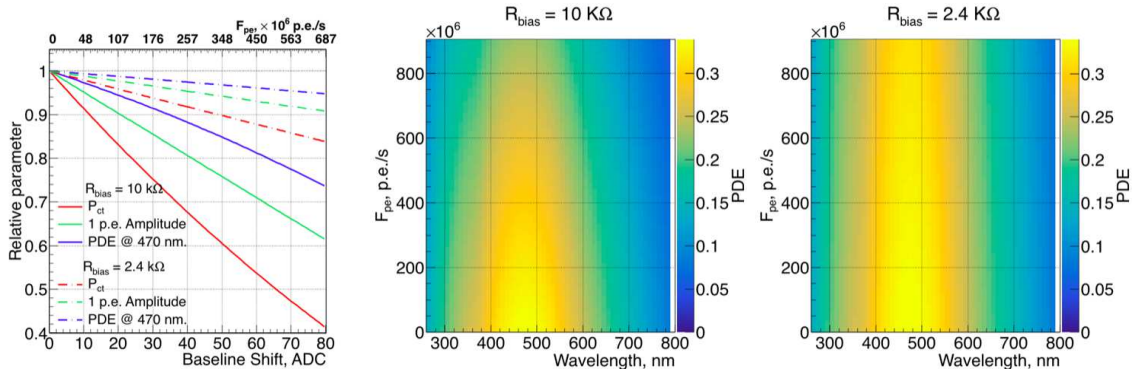


Figure 11: Top: Relative 1 p.e. Amplitude, P_{ct} and PDE as a function of CL rate (in p.e./s) and wavelength for two values of R_{bias} of 10 k Ω and 2.4 k Ω . The middle and right plots show for the two indicated R_{bias} values the PDE as a function of the CL rate in p.e. and wavelength.

The drop of the SiPM parameters (See Fig. 11) under CL may be compensated by increasing the bias voltage V_{SiPM} by some correction voltage V_{corr} in order to keep constant the over-voltage

ΔV (see Eq. 2.8). We call this “compensation loop”. V_{corr} is determined from the toy MC. As an example, the evolution of ΔV and V_{drop} with time under CL of 2×10^9 photons/s is shown with compensation loop (dashed lines) and without (solid lines) in Fig. 12 (top). We can observe that, to compensate by $V_{drop} \sim 0.9$ V, the V_{PS} should be increased by 1.7 V, as shown in Fig. 12 (bottom). As a drawback, the detected NSB rate increases from 505×10^6 p.e./s up to 653×10^6 p.e./s. Hence, the SiPM power consumption increased from 5.17 mW up to 10.29 mW.

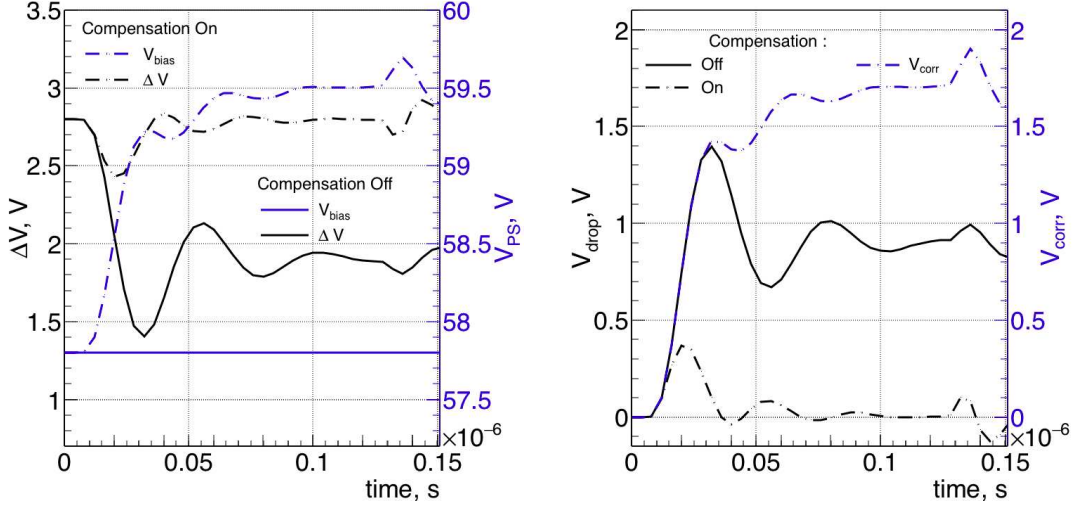


Figure 12: Evolution of over-voltage ΔV and V_{PS} averaged over 10'000 samples with time under a CL of 2×10^9 photons/s, with and without compensation loop (left). The voltage drop V_{drop} and the bias voltage correction V_{corr} are presented at the right.

The V_{corr} as a function of baseline shift is presented in Fig. 13 for two values of R_{bias} of 10 k Ω and 2.4 k Ω . We can observe that V_{corr} increases linearly with increasing baseline shift with a slope of $13.47 \frac{mV}{ADC}$ and $3.23 \frac{mV}{ADC}$ for R_{bias} of 10 and 2.4 k Ω , respectively. Therefore, in experimental conditions, when CL is known and stable in time, the effects from V_{drop} can be corrected. As a drawback, the SiPM power consumption increases after compensation loop activation, as shown in Fig. 13. Also, the baseline standard deviation BL_{σ} can be used to calculate V_{corr} . However, it is less precise since BL_{σ} shows stronger dependence on statistics and electronic noise.

7 Conclusions

In this paper we report on the studies of SiPM behaviour under CL. A Toy Monte Carlo model was developed for DC coupled electronics. This model is used to predict the behaviour of all relevant SiPM parameters (i.e. Gain, Photon detection efficiency, optical crosstalk, after-pulses, dark count rate and etc.) under various CL. The model is validated by comparison with experimental data measured for a single SiPM as well as for the full SST-1M gamma-ray camera, which contains 1296 SiPM devices. This model can be adapted to any DC coupled SiPM. Indeed, it can also be extended to the AC coupling case. As a matter of fact, in [5] it can be seen that the standard deviation of the

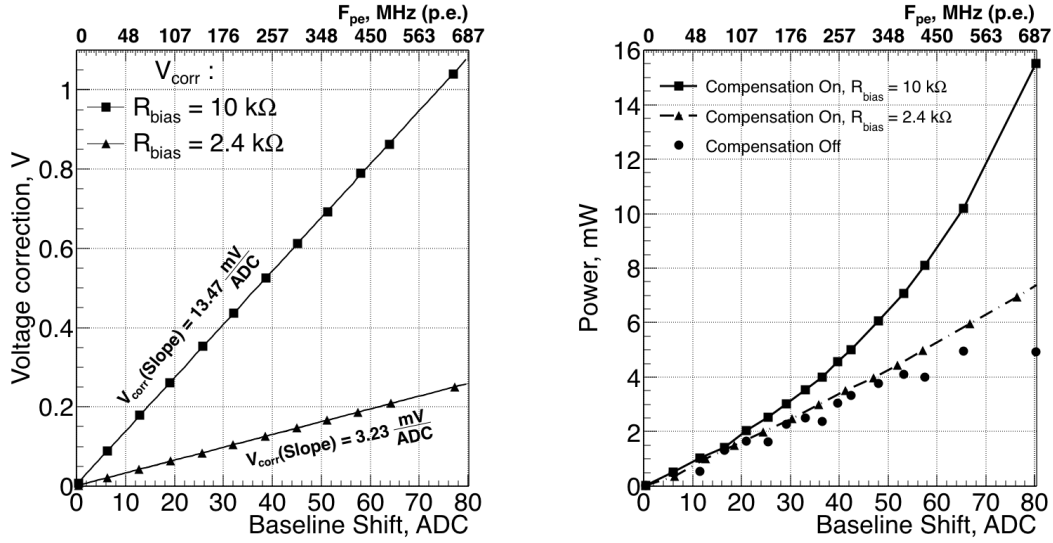


Figure 13: Correction bias voltage V_{corr} (left) that needs to be applied to have a constant over-voltage of $\Delta V=2.8\text{ V}$ as a function of the baseline shift for two values of R_{bias} of $10\text{ k}\Omega$ (rectangles) and $2.4\text{ k}\Omega$ (triangles). A linear behaviour of V_{corr} with the baseline shift is found with slope of 13.47 ($R_{bias} = 10\text{ k}\Omega$) and 3.23 mV/ADC ($R_{bias} = 2.4\text{ k}\Omega$). The sensor power consumption is also shown (right) On the right y-axis (in blue) the sensor power consumption is shown with the same symbols for the two bias resistors as before. The circles are the SiPM power consumption with no compensation loop.

waveform also increases with increasing CL. This parameter can therefore be used as an indicator for AC coupled systems, similarly to the baseline shift that we used for DC coupling. However, we showed that a DC couple system is preferable as the standard deviation tends to saturate at large CL levels while the baseline shift does not.

References

- [1] H. Anderhub, et al., *Design and Operation of FACT – The First G-APD Cherenkov Telescope*, JINST 8 (06) (2013) P06008–P06008. doi:10.1088/1748-0221/8/06/p06008.
- [2] CTA Observatory, <https://www.cta-observatory.org/>.
- [3] B. S. Acharya, et al., *Science with the Cherenkov Telescope Array*, WSP, 2018. arXiv:1709.07997, doi:10.1142/10986.
- [4] T. Montaruli, *The small size telescope projects for the Cherenkov Telescope Array*, PoS ICRC2015 (2016) 1043. arXiv:1508.06472, doi:10.22323/1.236.1043.
- [5] M. Heller et al., *An innovative silicon photomultiplier digitizing camera for gamma-ray astronomy*, The European Physical Journal C 77 (1) (2017) 47. doi:10.1140/epjc/s10052-017-4609-z.
- [6] D. Neise, et al., *FACT - Status and experience from five years of operation of the First G-APD Cherenkov Telescope*, Nucl. Instr. Meth. A 876 (01) 2017). doi:10.1016/j.nima.2016.12.053.

- [7] E. Garutti, Y. Musienko, *Radiation damage of SiPMs*, Nucl. Instrum. Meth. A 926 (2019) 69 – 84, silicon Photomultipliers: Technology, Characterisation and Applications.
[doi:https://doi.org/10.1016/j.nima.2018.10.191](https://doi.org/10.1016/j.nima.2018.10.191).
- [8] A. Para, *Afterpulsing in Silicon Photomultipliers: Impact on the Photodetectors Characterization* (2015). [arXiv:1503.01525](https://arxiv.org/abs/1503.01525).
- [9] Hamamatsu web site, <https://www.hamamatsu.com>, accessed: 2019-02-07.
- [10] A. Biland, et al., *Calibration and performance of the photon sensor response of FACT — the first G-APD Cherenkov telescope*, Journal of Instrumentation 9 (10) (2014) P10012–P10012.
[doi:10.1088/1748-0221/9/10/p10012](https://doi.org/10.1088/1748-0221/9/10/p10012).
- [11] A. Nagai, et al., *Characterization of a large area silicon photomultiplier*, Nucl. Instr. Meth. A 948 (2019) 162796. [doi:https://doi.org/10.1016/j.nima.2019.162796](https://doi.org/10.1016/j.nima.2019.162796).
- [12] J. Aguilar, et al., *The front-end electronics and slow control of large area SiPM for the SST-1M camera developed for the CTA experiment*, Nucl. Instrum. Meth. A 830 (2016) 219 – 232.
[doi:https://doi.org/10.1016/j.nima.2016.05.086](https://doi.org/10.1016/j.nima.2016.05.086).